Physics of Fluids

RESEARCH ARTICLE | MARCH 04 2024

Fingering of a cavitation bubble in a thin gap: Ejection of the reversed boundary layer into the bulk flow

Anna Borich ; Petr Denissenko

Physics of Fluids 36, 032001 (2024)
https://doi.org/10.1063/5.0184351

Physics of Fluids ARTICLE pubs.aip.org/aip/pof

Fingering of a cavitation bubble in a thin gap: Ejection of the reversed boundary layer into the bulk flow

Cite as: Phys. Fluids **36**, 032001 (2024); doi: 10.1063/5.0184351
Submitted: 25 October 2023 · Accepted: 1 February 2024 ·
Published Online: 4 March 2024

View Online Export Citation CrossMark

Anna Borich[1,a)] and Petr Denissenko[2]

AFFILIATIONS

[1]Department of Physics, Otto von Guericke University, Universitatsplatz 2, 39106 Magdeburg, Germany
[2]School of Engineering, University of Warwick, Coventry CV8 1GP, United Kingdom

[a)]Author to whom correspondence should be addressed: anneborich@gmail.com

ABSTRACT

The flow around a bubble, precipitously expanding in a thin gap between flat walls, was found to have a peculiar feature: distinct fingering occurs at the bubble wall, which was observed through the ultra-high speed optical visualization. The effect is attributed to the reversal of the flow within boundary layers, which provokes the growth of instabilities at the inflection point and, when the surface tension is low enough (the local Weber number is high enough), leads to the fingering. In this paper, we show the high speed recordings of the fingering and model the evolution of the radial velocity to quantitatively confirm feasibility of the proposed instability mechanism.

I. INTRODUCTION

Flows in squeezed confinements get an increased interest in recent decades. Structures associated with thin gaps, porous media, or micrometric-sized devices are relevant in multiple industrial and biomedical applications. Examples include petrol industry and related ground oil extrusion problems,[1] various tasks in microfluidic devices (cooling, material transport, etc.[2]), flows of biofluids, e.g., vascular or pulmonary systems,[3,4] and precision mixing in pharmaceutical production.

A common geometry to study multi-phase flows in thin gaps is a so-called Hele–Shaw cell, representing two parallel plates, squeezing one sort of liquid inside (for example oil), where one of the plates has an orifice for a controlled injection of another liquid (for example water). A common flow structure includes fingering of one liquid through another, when less viscous fluid is injected into a more viscous liquid (for example, water into an oil). In this paper, we report a visually similar but of a different physical mechanism pattern, observed in a time-dependent high Reynolds number flow at microscopic scale, that is, fingering at the edge of a cavitation bubble in a micrometer-sized gap.

II. EXPERIMENTAL ARRANGEMENT

The experimental setup is schemed in Fig. 1. A series of experiments was organized in a small scale Hele–Shaw cell. It is composed of two microscope coverslip slides (thickness 150 μm and dimensions $20 \times 20\,\text{mm}^2$), with water in between. A short laser pulse (7 ns, 0.2 mJ and λ 1064 nm) is focused in a thin (5–12 μm) gap filled with water. A dielectric breakdown occurs, inducing a sharp rise in pressure from the expanding plasma. That, in turn, creates a bubble experiencing a regular cavitation cycle of expansion and shrinking.

The rate of bubble expansion is higher than that of shrinking, and a fingering pattern appears at the outer boundary, visually similar to that of viscous fingering in two-phase Hele–Shaw flows.[5] The fingering represents a periodic structure at the gas–liquid interface, as shown in Fig. 2.

The overall process of interest takes no more than 3 μs and is captured with an ultra-high speed camera (5 Mfps, Shimadzu HPV-X2 with CMOS sensor), synchronized with illumination provided with a femtosecond pulsed laser (pulse duration 200 fs at a maximum repetition rate of 5 MHz, λ 515 nm, FemtoLux 3 SH EKSPLA).

III. EXPERIMENTAL OBSERVATIONS

A typical image sequence is shown in Fig. 2 (Multimedia view). Following the pulse of a focused laser beam (left bottom part of the image, marked with a dot owing to a slight glass damage), a bubble starts to expand radially, developing ripples at its walls, as clearly seen in all the images. An circular cloud of smaller bubbles distant from the main bubble are the secondary cavitation bubbles discussed later. When the gap between slides is thin enough (generally, below 10 μm), the outer boundary of the expanding bubble becomes unstable and finger-type protrusions of the gas bubble form. The fingers disappear

when the bubble contracts after reaching the maximum radius. When the gap is large (typically, above 10 μm), the outer boundary remains more or less circular and fingers do not form. A set of characteristic timeseries of the outer bubble boundary $r_b(t)$ and of the inner bound of the forming fingers is shown in Fig. 3. Note that normally fingers do not form in cases when the bubble expansion rates are lower, which occurs at higher gap heights. When the bubble growth nearly stops, fingers approach their maximum length and capillary forces become large enough to smooth the bubble boundary. A microsecond after the bubble contraction stops, the fingers disappear.

For the case represented in Fig. 2, the laser pulse energy of 0.2 mJ ($\lambda = 1064$ nm and pulse duration 7 ns in a gap thickness of $5 - 7$ μm) drives the fingers to reach the length 17 μm, with the width of 5 μm and liquid-filled distance between them of 5 μm. It is important to note that up to this point the characteristic spacing between the fingers grows with time and reaches approximately a half of the gap height.

IV. DISCUSSION

A. Estimates to the order of magnitude

We start explanation of fingers' formation by eliminating the terms in the governing equations, which are commonly associated with fingering but are negligible in our case. The quantitative values involved in the problem are as follows:

$$\begin{gathered}\text{water kinematic viscosity } \nu = 10^{-6}\ \mathrm{m^2 s^{-1}} \\ \text{water density} \rho = 10^3\ \mathrm{kg\,m^{-3}} \\ \text{water surface tension } \sigma = 0.72\ \mathrm{N\,m^{-1}} \\ \text{gap heighth} = 10\ \mu\mathrm{m} \\ \text{velocity of the bubble boundary when} \\ \text{fingers start forming } U_0 \sim 100\text{–}200\ \mathrm{m\ s^{-1}} \\ \text{deceleration of the bubble boundary when} \\ \text{fingers start forming } a_0 \sim 5\text{–}20 \times 10^8\ \mathrm{m\ s^{-2}}.\end{gathered}$$

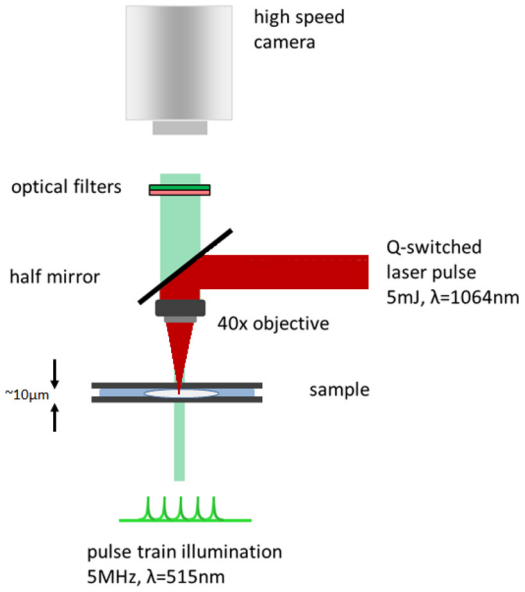

FIG. 1. Experimental setup: Laser generating a bubble is focused into a sample composed of two microscopic slides. The process is captured with ultra-high speed camera. Illumination is organized with the femtosecond laser in front of it.

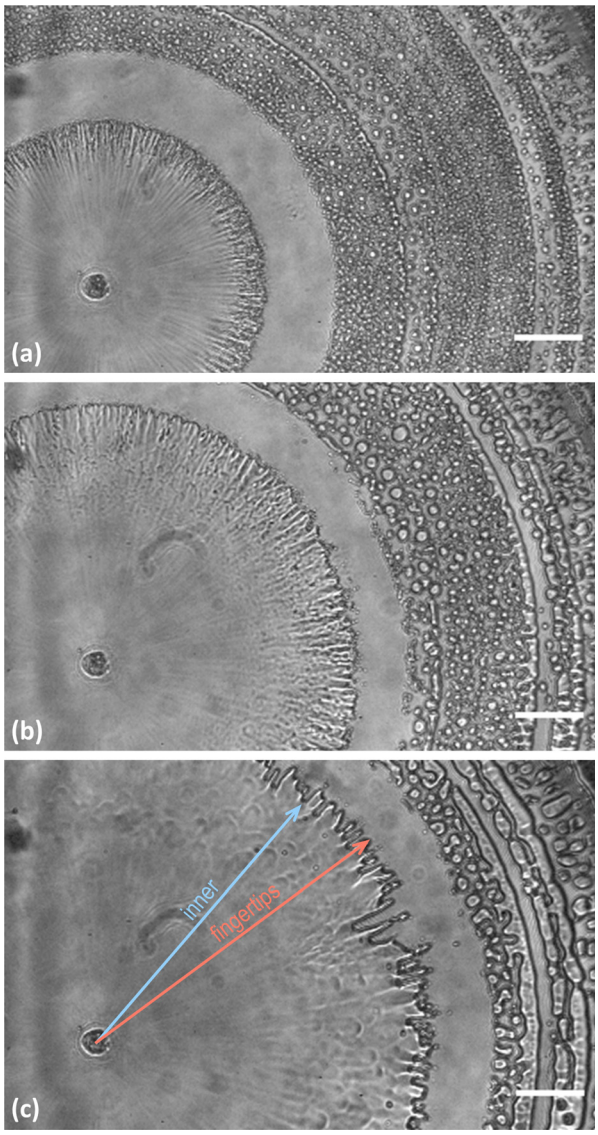

FIG. 2. Fingering at the outer boundary of a cavitation bubble in a thin gap. Images taken at (a) 200, (b) 600, and (c) 1400 ns after the laser pulse, see Fig. 3 for the corresponding data points. At the first image, the bubble boundary is nearly circular with ripples forming at liquid films at the gap walls. At the last image, fully formed fingers are seen. Outer dark area, distant from the main bubble, is filled with small secondary cavitation bubbles. Inner radius and "fingertips," indicated by blue and red arrows, have been approximately tracked. Scale bars are 50 μm. Multimedia available online.

The liquid is considered incompressible, and the gradients of radial velocity across the gap (z-direction) are much larger than the gradients in the radial direction.

The assumptions above lead to the following non-dimensional numbers:

$$\mathrm{Re} = \frac{hU_0}{\nu} \sim 1000\text{–}2000,$$

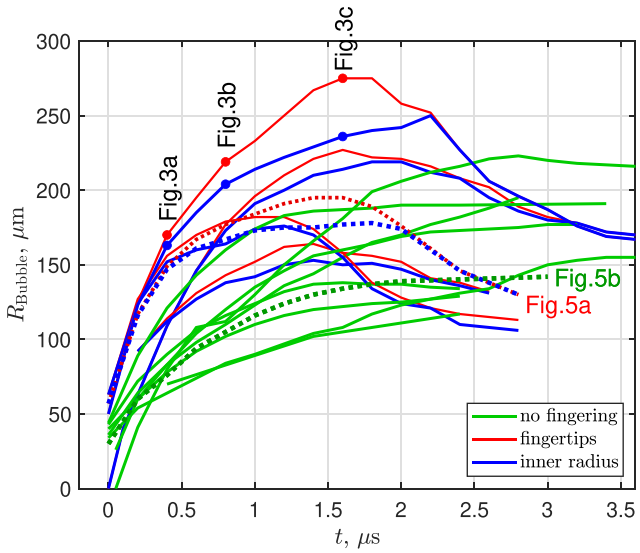

FIG. 3. Evolution of the bubble radius: experiments with and without fingering. Timeseries from 15 realizations are shown in the figure. Green lines correspond to cases with no fingering, and pairs of red and blue lines show radius of the "fingertips" and "interdigits" in experiments with fingering. We observe that usually fingers do not form in experiments with lower bubble expansion rates. Data points corresponding to the frames shown in Fig. 2 are indicated by the black text. Data series corresponding to the experiments used for simulation of velocity profiles with and without fingering in Fig. 5 are indicated by red and green text, respectively.

which suggests the flow in the gap is of a boundary-layer type, with the flow in the midgap being a z-independent flow driven by inertia and the radial pressure gradient, as later confirmed by simulations shown in Fig. 6. The values related to capillary forces are Capillary, Eötvös, and Weber numbers:

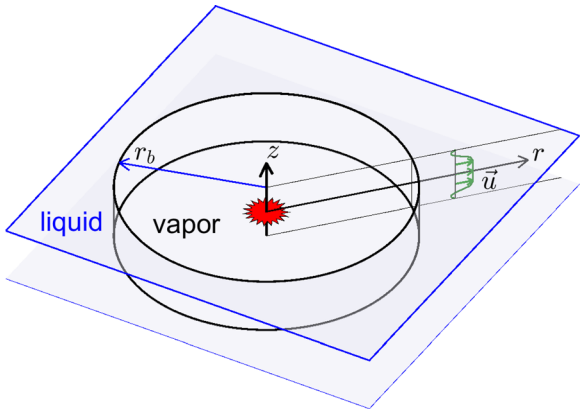

FIG. 4. Geometry of the axisymmetric flow around the cavitation bubble, with z axis is directed across the channel. The bubble radius is r_b, the profile of the fluid velocity is indicated by the green line, and the focal point of the bubble-generating IR laser in the midgap is indicated by the red star.

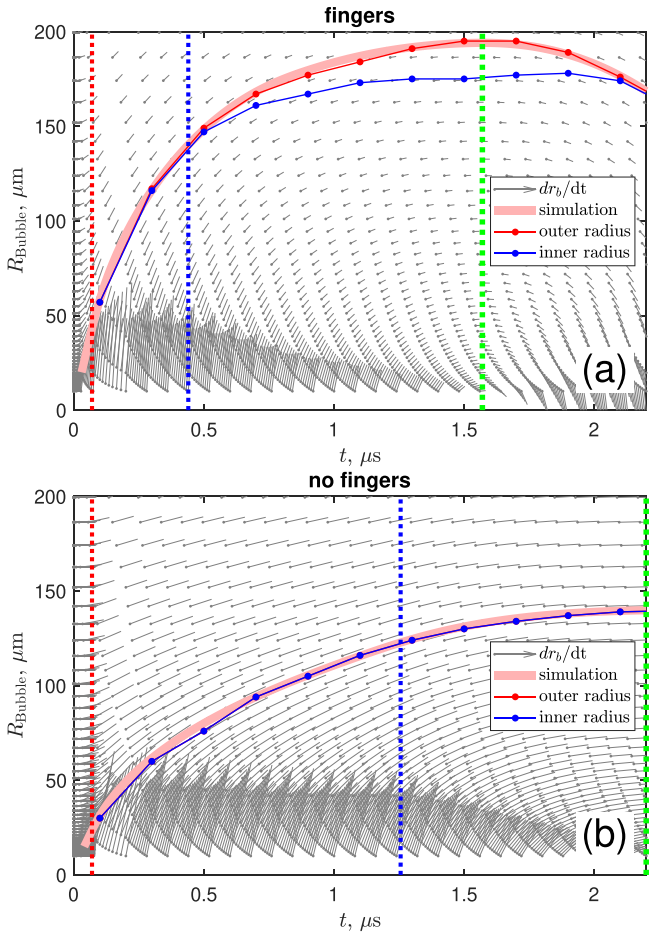

FIG. 5. Evolution of the bubble radius $r_b(t)$: experiment (lines with markers) and simulation (solid line); (a) corresponds to the case with fingering forming and (b) shows the case where the bubble remains circular. Gray segments show the direction field dr_b/dt of the ODE (4) used to simulate $r_b(t)$. The red dotted line shows the time instant of the inversion of pressure gradient, the dotted blue line shows the time instant when the radial velocity near walls changes sign (see profiles in Fig. 6), and the green dotted line marks the instant when the bubble stops expanding.

$$\text{Ca} = \frac{\nu\rho U_0}{\sigma} \sim 1\text{–}2,$$
$$\text{Eo} = \frac{\rho a_0 h^2}{\sigma} \sim 1000\text{–}3000,$$
$$\text{We} = \frac{\rho U_0^2 h}{\sigma} \sim 150\text{–}600,$$

which suggests that surface tension can only compete with viscous forces and plays role in the "corners" of the cylindrical-shaped bubble and do not affect the dynamics of its side walls. We later observe (Fig. 6) that the local Weber number, based on the distance from a boundary rather than on the gap height, can become small and hence fingers do not form.

Formation of the fingers is, therefore, guided by the flow deceleration and processes in the near-walls boundary layer, i.e., mechanisms completely different from those responsible for the visually similar viscous fingering in Hele–Shaw configuration.

B. Evolution of the radial velocity

Without discussing the flow structure in liquid layers between the bubble and gap walls, i.e., at radii below the radius of the bubble $r < r_b$, we model the evolution of radial velocity profiles in the water-filled part of the gap, at $r > r_b$, outside the bubble (see schematic in Fig. 4). Assuming that the only velocity component is radial $u(r, z)$ and the flow is axisymmetric and incompressible, the continuity equation gives

$$\frac{\partial}{\partial r}(r\ u) = 0, \tag{1}$$

which yields

$$u \propto r^{-1}. \tag{2}$$

In accordance with the assumptions above and noting that dimensions across the gap are an order of magnitude smaller than those in the radial direction, $\frac{\partial^2 u}{\partial z^2} \gg \frac{\partial^2 u}{\partial r^2}$, and therefore, Navier–Stokes equations for radial velocity are as follows:

$$\frac{\partial u}{\partial t} = \nu \frac{\partial^2 u}{\partial z^2} - \frac{1}{\rho}\frac{\partial P}{\partial r} + \frac{u^2}{r}. \tag{3}$$

Here, P is the pressure along the streamline, r-radial distance, and z-coordinate in the normal to the walls direction, across the gap.

As seen in Fig. 2, a torus cloud of small bubbles also forming ahead of the larger, laser-induced, bubble boundary. These are so-called secondary cavitation bubbles generated by the Lamb wave passage at the walls interface.[6] The group dynamics of these interacting bubbles and deformation of the gap walls creates a complex pressure gradient $\frac{\partial P}{\partial r}$.

In order to determine it, we find the timeseries $\frac{\partial P}{\partial r}(t)$ in the following way. First, the equation is solved numerically at a given radius with an arbitrary assigned pressure gradient $\frac{\partial P}{\partial r}(t)$. The non-slip boundary conditions are chosen at walls and zero velocity is chosen at $t = 0$. Then, we use the value of $u(r, z, t)$ in the middle of the gap $z = 0$ and the continuity (2) to get the direction field for the evolution of the bubble radius:

$$\frac{dr_b}{dt} = u(r_b, 0, t). \tag{4}$$

At that point, we solve the ODE (4) numerically with the initial conditions taken from Fig. 3 and manually tune $\frac{\partial P}{\partial r}(t)$ to match the experimentally observed $r_b(t)$, as shown in Fig. 5. Obtained profiles of the radial velocity at the radius where fingers start forming (150 μm) are plotted in Fig. 6 at different time instants. The red line shows the time instant of the reversal of the pressure gradient, which happens shortly after the flow deceleration starts. The blue line shows time instant where the fingers start forming (0.5 μs), and the green line corresponds to the time when the bubble radius stops growing, i.e., velocity in the midgap reaches zero. Note that when the gap is wide, boundary layers (and hence regions where the flow is reversed) do not occupy a notable part of the gap, hence the fingers do not form.

The high pressure gradient $\frac{\partial P}{\partial r} \sim 10^{11}$ Pa/m decelerating the flow may occur due to the combination of the Leaky Rayleigh wave, which travels with a speed ~ 3250 m/s and the bulk wave in glass, which travels at ~ 5000 m/s.

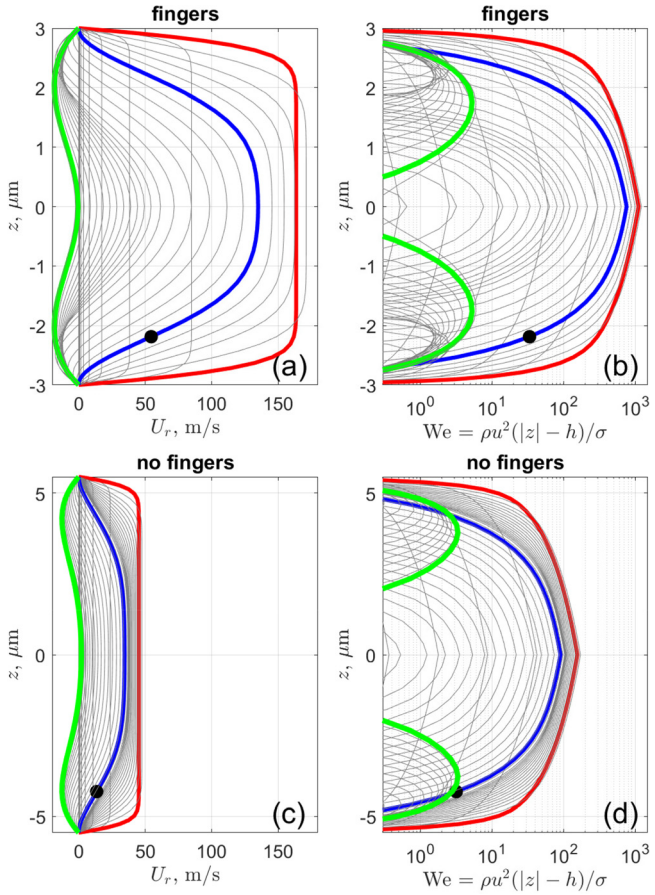

FIG. 6. Profiles of radial velocity (a) and (c) and local Weber number across (b) and (d) the gap (see the velocity profile in Fig. 4 for illustration). For the fingers to form, boundary layers should occupy a notable part of the gap. Following the laser pulse, the fluid accelerates due to the positive pressure gradient, forming boundary layers; the red line corresponds to the time instant where the pressure gradient changes sign. Following the reversal of the pressure gradient, the flow in the bulk decelerates while the flow in the near-wall boundary layers reverses; the corresponding time instant is shown by blue lines. In the case with fingering (a), this approximately coincides with the time of finger formation, i.e., when the outer and inner radii of the bubble boundary start differing as shown in Fig. 5. Black dots indicate the distance from wall where velocity decreases e times compared to velocity in the midgap, which can be interpreted as the edge of the boundary layer. When the flow in midgap stops (green lines), the bubble growth stops while strong inward flow already exists near gap walls. The mentioned time instants are marked by dotted lines in Fig. 5.

C. Mechanism of the finger formation

The evolution of the bubble radius is shown in Fig. 5, for the cases when the fingering forms and does not form. Following the laser pulse, the bubble expands with the maximum expansion rate up to 500 m/s. This stage spans first few tens nanoseconds and is not resolved by the camera. At this stage, the Reynolds number based on the gap height reaches 5000. With inertial effects dominating, the thickness of near-wall boundary layers does not exceed a diffusion propagation distance $\sqrt{\nu\tau} \sim \sqrt{10^{-6} \times 200 \times 10^{-9}} \sim 0.5\ \mu$m, as confirmed by simulation shown by red lines in Fig. 6.

Then, the reverse pressure gradient decelerates the bulk flow while the flow in boundary layers stops and then reverses as observed in a number of configurations[7,8] and shown by blue and green lines in Fig. 6 and schematically illustrated in Fig. 7.

As the resulting flow profile has an inflection point, it becomes unstable with annular vortices forming at the edge of the boundary layer. These vortices are then stretched in the streamwise direction in a way common in wall-bounded shear layers.[9,10] Forming streaks, known as coherent structures in the near wall shear flow, lead to ejections of the slow-moving liquid into the bulk flow, which manifests in the radial inhomogeneities in the thickness of the liquid film, appearing as bright radial stripes near the bubble boundary, seen in Figs. 2(a) and 2(b). The spatial distance between the streaks is of the order of 2 μm, which is consistent with the dimension of near-wall layers of low radial velocity, seen in Fig. 6. As the liquid decelerates further, the magnitude of reverse flow becomes comparable with the velocity in the bulk, the boundary layers grow, the ejections of the reversed flow span the whole gap, and the fingers form. The spacing between fingers is therefore comparable with the gap height, as seen in Fig. 2(c). In the experiments where the gap height is larger, the flow is slower, and the surface tension hinders the development of the fingers, which can be illustrated by the 10-fold decrease in the Weber number in Fig. 6(d) compared to Fig. 6(b).

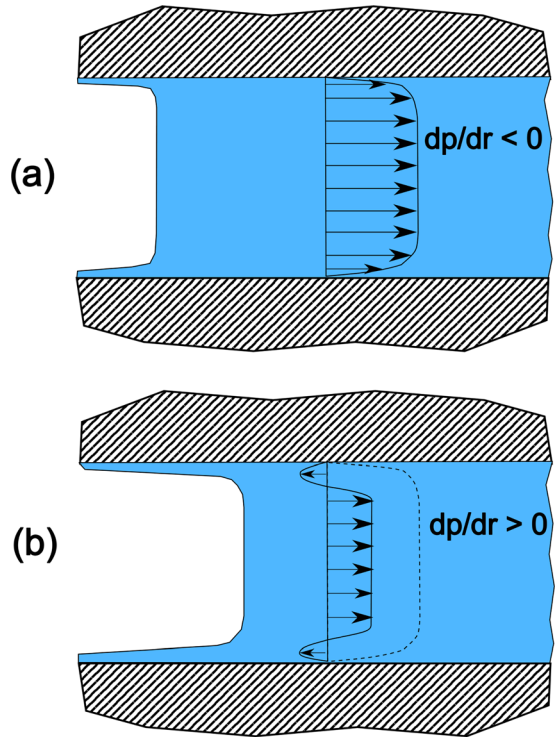

FIG. 7. Following the laser pulse, the fluid accelerates due to the negative radial pressure gradient (a). When the pressure gradient reverses, the flow in the bulk decelerates, while the flow in the near-wall boundary layers reverses (b), compared with modeled profiles shown in Figs. 6(a) and 6(c).

V. CONCLUSION

We have presented observations of peculiar instabilities, namely, sharp fingers, forming at the outer boundary of a rapidly expanding bubble in a thin gap. Due to high dynamic pressures involved, the mechanism of the fingering is completely different from that in visually similar pressure-driven Hele–Shaw configurations. To explain the fingering, we have simulated radial velocity of the liquid outside the bubble, revealing the presence of an inflection in the cross-gap velocity profile. The inflection causes instability with ejection of reversed flow from the wall-bounded boundary layer. That, in turn, manifests in formation of radial inhomogeneities, which develop into distinct fingering.

ACKNOWLEDGMENTS

The authors wish to acknowledge the Soft Matter laboratory of Otto von Guericke University for the opportunity to conduct the experimental part of the work.

AUTHOR DECLARATIONS

Conflict of Interest

The authors have no conflicts to disclose.

Author Contributions

Anna Borich: Conceptualization (equal); Data curation (equal); Formal analysis (equal); Funding acquisition (equal); Investigation (equal); Methodology (equal); Project administration (equal); Resources (equal); Software (equal); Supervision (supporting); Validation (supporting); Visualization (equal); Writing – original draft (equal); Writing – review & editing (equal). **Petr Denissenko:** Conceptualization (equal); Data curation (equal); Formal analysis (equal); Funding acquisition (equal); Investigation (equal); Methodology (equal); Project administration (equal); Resources (equal); Software (equal); Supervision (lead); Validation (lead); Visualization (equal); Writing – original draft (equal); Writing – review & editing (equal).

DATA AVAILABILITY

The data that support the findings of this study are available from the corresponding author upon request.

REFERENCES

[1]P. G. Saffman and G. I. S. Taylor, "The penetration of a fluid into a porous medium or Hele-Shaw cell containing a more viscous liquid," Proc. R. Soc. London, Ser. A **245**, 312–329 (1958).
[2]L. Delon, Z. Guo, M. N. Kashani, C.-T. Yang, C. Prestidge, and B. Thierry, "Hele Shaw microfluidic device: A new tool for systematic investigation into the effect of the fluid shear stress for organs-on-chips," MethodsX **7**, 100980 (2020).
[3]D. Huh, H. Fujioka, Y.-C. Tung, N. Futai, R. Paine, J. B. Grotberg, and S. Takayama, "Acoustically detectable cellular-level lung injury induced by fluid mechanical stresses in microfluidic airway systems," Proc. Natl. Acad. Sci. U. S. A. **104**(48), 18886–18891 (2007).
[4]J. Grotberg and O. Jensen, "Biofluid mechanics in flexible tubes," Annu. Rev. Fluid Mech. **36**, 121 (2004).
[5]L. Paterson, "Radial fingering in a Hele Shaw cell," J. Fluid Mech. **113**, 513–529 (1981).
[6]J. Rapet, P. Quinto-Su, and C.-D. Ohl, "Cavitation inception from transverse waves in a thin liquid gap," Phys. Rev. Appl. **14**, 024041 (2020).

[7]P. Hall, "Unsteady viscous flow in a pipe of slowly varying cross-section," J. Fluid Mech. **64**(2), 209–226 (1974).
[8]J. T. Stuart, "Double boundary layers in oscillatory viscous flow," J. Fluid Mech. **24**(4), 673–687 (1966).
[9]S. K. Robinson, "Coherent motions in the turbulent boundary layer," Annu. Rev. Fluid Mech. **23**(1), 601–639 (1991).
[10]S. K. Robinson, "The kinematics of turbulent Boundary layer structure," NASA Technical Memorandum No. 103859, 1991.